Semiconductor Physics, Quantum Electronics & Optoelectronics, 2006. V. 9, N 3. P. 4-11.

PACS 43.35Cg, 43.35Zc, 43.35Ns

Microacoustic evaluation of elastic parameters of highly porous silicon layers

A. Doghmane[1], Z. Hadjoub[1], M. Doghmane[1,2], F. Hadjoub[1,3]
[1]*Laboratoire des Semiconducteurs, Département de Physique, Faculté des Sciences, Université Badji-Mokhtar, BP 12, Annaba, DZ-23000, Algeria*
[2]*Faculté des Sciences et de l'Ingénierie, Université du 8 Mai 1945, Guelma, DZ-24 000, Algeria*
[3]*Faculté de Médecine, BP 205, Annaba DZ-23 000, Algeria*
E-mail : a_doghmane@yahoo.fr

Abstract. Non-destructive scanning acoustic microscopy investigations of elastic properties of porous silicon films, limited to low and medium porosities, are extended in this work to higher porosities (80 %) corresponding to the appearance of room temperature electroluminescence phenomena. Acoustic materials signatures were measured at various operating frequencies, f, and film thickness, d. It was shown that as these parameters increase the oscillatory $V(z)$ behaviour disappears progressively to become completely attenuated, for f = 565 MHz and d = 6 µm, due to wave absorption, with α_x = 0.2 µm^{-1}. Moreover, from high frequency microechography, it was possible to determine longitudinal velocity, V_L = 1680 m/s. To evaluate Young's modulus, E, and shear modulus, G, we used two different approaches to derive simple expressions for these constants in terms of just V_L. The validity of such expressions was successfully put into evidence then applied to the highly porous silicon layers for which it was found that E = 1.29 GPa and G = 0.63 GPa.

Keywords: porous Si, elastic constants, electroluminescence, acoustic microscopy, surface acoustic wave.

Manuscript received 08.02.06; accepted for publication 29.03.06.

1. Introduction

Crystalline, microcrystalline and amorphous silicon have been playing a very important role in many aspects of fundamental and applied research fields as a result of the well established and relatively cheap technology of this semiconductor element. However, with an energy gap of 1.1 eV, silicon remained up till recently unapplied into optoelectronics, which was reserved to compound semiconductors technologies of which are relatively difficult and, usually, very costly. The discovery of visible electroluminescent phenomenon in porous silicon (PS) even at room temperature (RT) [1, 2] stimulated a great deal of interest [3, 4]. With an energy gap of 0.5 eV greater than its crystalline counterpart [5], this semiconductor opened up many other application fields [6, 7] such as opto-, micro-, and nanoelectronics. However, RT electroluminescence phenomenon, in such a material, can only be observed when its porosity reaches a high level of about 80 %. This high porosity level makes it very fragile, and hence the investigation of its elastic properties, which are important parameters, more delicate. Recently, great efforts have been devoted to the investigation of elastic properties of PS films using X-ray diffraction [8], acoustic microscopy techniques [9-11], nanoindentation and Brillouin spectroscopy [12-16]. However, only few Young's modulus values have been reported in the literature for PS films with even less investigations for high porosity films. In fact, even the scanning acoustic microscopy method [17-19], which is one of the most challenging tools for non-destructive testing has only been applied to low and medium porosity films of less than 50 % [9-11].

It is the aim of this work to extend microacoustic investigation methods to highly porous silicon, H-PS, layers. In doing so, we first measure the acoustic material signatures at various operating frequencies and film thicknesses via a scanning acoustic microscope (SAM). Then, we measure the longitudinal wave velocity, V_L, of such layers. Finally, using different acceptable approximations we derive an elastic constants formula as a function of only V_L, then determine the most accurate expressions to evaluate both elastic moduli of such H-PS layers.

© 2006, V. Lashkaryov Institute of Semiconductor Physics, National Academy of Sciences of Ukraine

2. Background on porosity effects on acoustic parameters

The investigation of porosity is of great importance in the determination of materials characteristics. Among the most challenging characterisation techniques of thin films, coating and bulk materials are ultrasonic non-destructive evaluation methods, involving the measurements of wave velocities. Hence, the acoustic parameters that can be investigated are transverse, longitudinal and Rayleigh velocities (V_T, V_L and V_R, respectively), longitudinal impedance, Z_L, transverse impedance, Z_T, and elastic constants (Young's modulus, E, and shear modulus, G). Several attempts concerning the dependence of porosity, P, on single or on some of these acoustic parameters were previously reported in connection with some materials. It was first reported that [20] ultrasonic velocity and Young's modulus are related to porosity by the following expressions:

$$V = V_0(1 - P)^m, \tag{1a}$$

$$E = E_0(1 - P)^n, \tag{1b}$$

where the subscript ($_0$) stands for non-porous materials and the empirical constants m and n depend on the microstructure with $m = 1.009$ for a porous brittle solid [20]. Such dependences were also recently reported for porous silicon with $m = 1.095$ [11] and $n = 2.93$ [13]. Other dependences, for low porosities ($P \le 10$ %), were expressed as [21, 22]:

$$V = V_0(1 - \alpha P)^m, \tag{2a}$$

$$(E, G) = (E_0, G_0)\exp(\alpha P + \beta P^2), \tag{2b}$$

where α and β are characteristic empirical constants describing the variation of each parameter.

A more general and improved investigation [9], using the scanning acoustic microscopy method, was recently reported on the porosity effects on several measured acoustic parameters, $A \equiv V_L$, V_R, V_T, Z_L, Z_T, E or G in silicon films of low and medium porosities (≤ 50 %). It was found that all such parameters give a similar polynomial dependence of the form:

$$A = A_0(1 - \alpha P + \beta P^2), \tag{3}$$

where A_0 is the non-porous acoustic parameter representing: V_{L_0}, V_{R_0}, V_{T_0}, Z_{L_0}, Z_{T_0}, E_0 or G_0. The values of the empirical constants α and β are typical of each individual acoustic parameter.

The importance of knowing acoustic parameters, in particular surface acoustic wave (SAW) velocities, lies in their use to non-destructive determination of both E and G; these elastic moduli are given, according to physical acoustics theory, for any given material of density, ρ, by the following relations:

$$E = \rho V_T^2 \frac{3 - 4\left(V_T/V_L\right)^2}{1 - \left(V_T/V_L\right)^2}, \tag{4}$$

$$G = \rho V_T^2. \tag{5}$$

3. Experimental details

3.1. Porous silicon films

Porous silicon films are obtained by electrochemical dissolution of monocrystalline silicon in concentrated hydrofluoric acid HF solutions (10 to 40 %). The application of d.c. current between the silicon electrode and a cathode generates an array of extremely small holes width range of which from 2 to 20′; these pores run orthogonal to the surface to form a thin PS film within the upper surface of the silicon substrate. The density and the dimension of such quasi-cylindrical pores are dependent on the preparation conditions. The porous films obtained are then oxidized, using aqueous solutions (HCl or KNO_3) in the same electrochemical cell at constant small current densities of order of the mA/cm^2. During this anodic oxidation a red orange colour is observed on the wafer surface. It is worth noting that this electroluminescence phenomenon depends on the degree of porosity as well as on the oxidation time, t [23]; it begins to appear at $t \approx 0$ for 85 % porosity samples and reaches its maximum at $t \approx 50$ s. Whereas, for 75 and 65 % porosity specimens it does not appear until 160 and 250 s, respectively, with intensities very much lower than those of 85 % porous silicon.

3.2. Quantitative acoustic investigations

Non-destructive acoustic investigations are based on the emission and reception of SAWs that interact with the elastic properties of a given material where different modes propagate. Among the most promising tools that have demonstrated a variety of unique capabilities in qualitative and quantitative characterisation of surface and sub-surface details are scanning acoustic microscopes. Such microscopes consist of several elements (Fig. 1); a piezoelectric transducer generates surface waves that propagate into a delay line, other end of which contains a lens that focuses these acoustic beams, through a coupling liquid, into the surface or at the sub-surface of the sample. Such beams, after having scanned the desired plane of the sample are reflected back following the inverse path (coupling liquid, lens, delay line) to be collected by the same initial transducer that acts now as a receiver.

In microanalysis, the output signal is recorded as the distance between the sample and acoustic lens is changed to obtain the $V(z)$ curves. Constructive and destructive interference between surface modes lead to the appearance of peaks and dips in such curves also known as acoustic materials signatures. Spectral analysis of these curves via fast Fourier transform treatment leads to the determination of the phase velocity, V_p, of the leaky SAWs from the special period, Δz, between two successive peaks (or two successive dips) in the $V(z)$ curves; it is given by the following relation [24]:

© 2006, V. Lashkaryov Institute of Semiconductor Physics, National Academy of Sciences of Ukraine

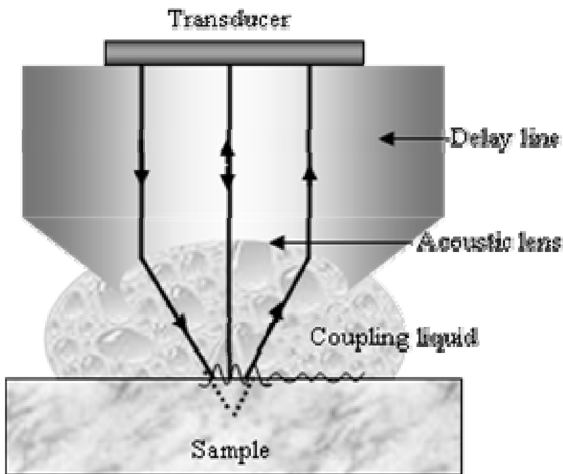

Fig. 1. Schematic representation of a scanning acoustic microscope.

$$V_p = \frac{V_{\text{liq}}}{\sqrt{1-\left(1-\frac{V_{\text{liq}}}{2f\,\Delta z}\right)^2}} \quad (6)$$

where V_{liq} is the longitudinal velocity in the coupling liquid and f is the operating frequency.

It should be noted that ultrasonic velocities, V, of propagating modes can also be determined via high frequency microechography techniques [11, 25] that are based on measuring the time interval Δt, between two reflected echoes from two interfaces of known spacing, d. The velocity is then given by the familiar relation: $V = 2d/\Delta t$.

3.3. Experimental conditions and materials

All experimental measurements of acoustic material signatures, $V(z)$ curves, were carried out via a scanning acoustic microscope, working in reflection mode, under normal operating conditions: water coupling and a 50° half-opening angle. Different operating frequencies, f, (58, 142 and 565 MHz) were considered. Using the configuration of highly porous films/crystalline Si substrates, n- and p-type Si ⟨100⟩ samples were investigated on both porous and crystalline sides. To study the effects of film thickness on $V(z)$ responses, thin (1 µm) as well as thicker H-PS layers (4 and 6 µm) were considered. High frequency microechography was applied, to determine longitudinal wave velocity at 200 MHz with mercury as a coupling liquid.

4. Experimental $V(z)$ curves and discussions

4.1. Frequency effects on V(z) signatures

Fig. 2 illustrates typical experimental $V(z)$ curves obtained by means of a SAM at f = 58 MHz (a), 142 MHz (b) and 565 MHz (c) for H-PS films/Si configurations (…) with a thickness of 1 µm of the H-PS layer; the continuous curves (——) represent bulk p-type c-Si substrates, to be considered as a reference curve. The use of such relatively and increasingly operating frequencies has the advantage of a good resolution in the z direction, thus allowing investigations of relatively thin specimens without interference effects of back side echoes. It is clear that the usual oscillatory behaviour of $V(z)$ response is clearly displayed for crystalline Si; in this case the conventional procedure [24, 26] (fast Fourier analysis and relation (6)) can safely be used to determine its Rayleigh velocity that was found to be $(V_R)_{Si}$ = 5160 m/s, in good agreement with literature [9, 10]. However, the $V(z)$ curves obtained for the H-PS film are characterised by a smaller signal amplitude that decreases continuously when the operating frequency increases. Thus, leading to period broadening and eventually the oscillatory behaviour becomes less pronounced.

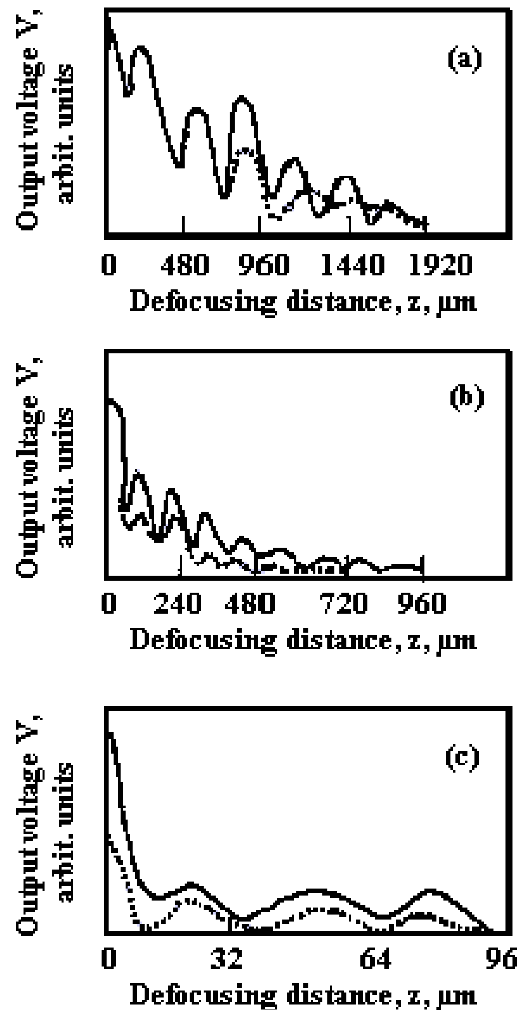

Fig. 2. Experimental $V(z)$ curves for the structure H-PS(1 µm)/Si substrate (…) and for bulk p-type Si substrate (——) obtained with SAM at variuos frequencies: f = = 58 MHz (a), 142 (b) and 565 (c).

© 2006, V. Lashkaryov Institute of Semiconductor Physics, National Academy of Sciences of Ukraine

The use of low frequencies would be sensitive to back reflection from the substrate, which may dominate and obscure the presumably porous silicon signatures. Therefore, in Fig. 2a, the $V(z)$ dotted curve (**…**) obtained at 58 MHz represent, in fact, the whole structure thin film/substrate [27, 28] rather than that of the 1 µm-porous Si layer. Hence, the velocity extracted from such curves does not represent necessarily that of H-PS films. The use of higher frequencies (Fig. 2c) leads smaller amplitudes and limits the number of arches as a result of the small defocusing distance. However, since the considered thickness is too small (1 µm), the remaining few periodic oscillations (**…**) still represent the whole H-PS/Si structure dominated by the c-Si substrate characteristics rather than those of porous films alone. Therefore, it is necessary to consider thicker specimens.

4.2. Thickness effects on V(z) signatures

To put into evidence film thickness effects on acoustic signatures, we measured other H-PS/c-Si structures with thicker layers at various operating frequencies (58, 142, and 565 MHz). Fig. 3 shows some typical experimental $V(z)$ curves obtained, at a frequency equal to 565 MHz, for relatively thicker (6 µm) porous samples (…) together with 1-µm H-PS/c-Si structure (- - -) and c-Si substrate (──). It can be seen that as the thickness of H-PS films increases we notice (i) a decrease in amplitudes, (ii) a broadening of the periods and (iii) a complete disappearance of the usual oscillatory behaviour of $V(z)$ curves for the highest thickness.

Therefore, it remains difficult to find a compromise between d and f in order to determine the values of propagating wave velocities of H-PS thick films from such curves. Nevertheless, from the measured $V(z)$ curves one can conclude, qualitatively, that as the film thickness increases the wave absorption increases leading the complete disappearance of peaks and valleys in $V(z)$ signatures. This behaviour is analogous to that of a plane monofrequency wave travelling in the z direction; the expression for the acoustic signal including absorption effects can be written as $V(z) = V_0 \exp(-\alpha_x z)$ with V_0 being the acoustic signal intensity at distance $z = 0$ and α_x the exponential decay. Therefore, from the $V(z)$ free oscillation curves it is possible to determine the attenuation coefficient that is related to the exponential decay [24, 29, 30]. Hence, from the fitting of the completely attenuated curve of Fig. 3, one can easily deduce a quantitative value for $\alpha_x = 0.2\ \mu m^{-1}$ for the 6-µm H-PS layer at a frequency of 565 MHz; further investigations on attenuation effects are underway.

5. Longitudinal wave velocity determination

In order to enrich and to complete the above SAM investigations for SAW velocity determination, we investigate longitudinal waves that can be generated in the material [10, 21]. It should be noted that the empirical formula (relation (3)) proposed for medium porosity films cannot be applied to the present 80 % PS layers, as it gives false results; a quick test shows some anomalous values in elastic constants, *e.g.*, shear modulus of 80 % PS is found to be abnormally greater than that of 50 % PS films. Hence, the alternative would be the use of the non-destructive high frequency microechography technique [11, 25] that seems to be suitable for these highly porous films.

Fig. 4 illustrates an equivalent pulse echo (amplitude versus time) for a structure of porous silicon film on a crystalline silicon, c-Si, wafer. The echoes were obtained at (i) a frequency of 200 MHz, which allows the separation of the reflected signals at the various interfaces and (ii) with mercury as a coupling liquid to ensure good wave transmission. In this configuration, the ultrasonic wave was chosen to fall on the back side of the c-Si substrate, in order to avoid the coupling liquid penetration in the porous silicon layer. Therefore, the first echo corresponds to the reflection from the Hg/c-Si interface surface. Whereas, the second

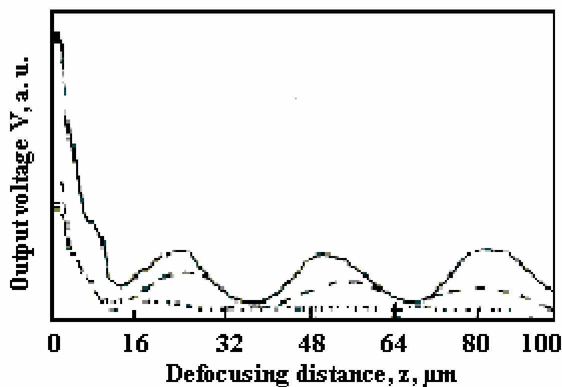

Fig. 3. Experimental $V(z)$ curves obtained with SAM at $f = 565$ MHz for bulk Si substrate (──), H-PS(1 µm)/Si structure (- - -) and H-PS(6 µm)/Si configurations (…).

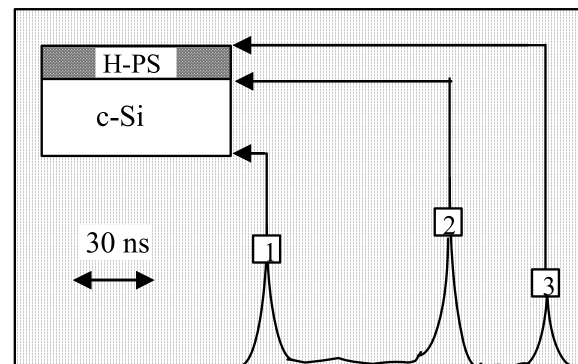

Fig. 4. Equivalent pulse echoes for different interfaces: liquid (Hg)/c-Si (1), c-Si/H-PS (2) and H-PS/free surface (3), obtained with $f = 200$ MHz.

© 2006, V. Lashkaryov Institute of Semiconductor Physics, National Academy of Sciences of Ukraine

and the third peaks correspond to reflections from c-Si/H-PS interface and from PS free surface, respectively. Hence, from the typical echoes displayed in the microechographic spectrum of Fig. 4, it can be deduced that longitudinal velocities for c-Si and H-PS films are $(V_L)_{c-Si}$ = 8433 m/s and $(V_L)_{H-PS}$ = 1680 m/s, respectively. Similar values were also found for other identical samples for this highly porous silicon.

6. Elastic constants determination

Highly porous silicon films are very fragile materials. Therefore, the determination of their elastic constants by conventional static methods is very delicate. Hence, the alternative would be ultrasonic non-destructive evaluation techniques requiring wave velocity measurements. However, due to difficulties in getting valuable information concerning the velocities of different propagating modes from SAM measurements, we make use of the measurement possibility via high frequency microechography of longitudinal velocity to express conventional relations (4) and (5) in terms of just the only measurable parameter, V_L.

6.1. Derivation of one-parameter formula for elastic constants

6.1.1. Approach based on the Viktorov formula

In deriving E and G in terms of just V_L, we make some acceptable approximations to the most widely known Viktorov formula [31]:

$$\frac{V_R}{V_T} = \frac{0.718 - 4\left(V_T / V_L\right)^2}{0.75 - \left(V_T / V_L\right)} . \qquad (7)$$

It should be noted that for the permissible range of the Poisson ratio from 0 to 0.5, over which V_T/V_L ranges from $1/\sqrt{2}$ to 0, the Rayleigh velocity varies from 87 to 95 % of transverse velocity [18]. Therefore, to a first approximation, it is usually considered that $V_R/V_T \approx 0.9$ [18, 27]; introducing this value into the left hand side of equation (7) leads to $(V_T/V_L)^2 \approx 0.43$. Then, we replace V_T^2 in the relations (4) and (5) to find novel expressions for E and G of the form:

$$E = 0.966\rho V_L^2 , \qquad (8)$$

$$G = 0.43\rho V_L^2 . \qquad (9)$$

6.1.2. Specific approach for porous silicon

To improve the above approach, we no longer consider the conventional approximation concerning the whole range of materials, *i.e.* $V_R \approx 0.9V_T$, but we use the relation: $V_R = C_{RT}V_T$, where C_{RT} is the proportionality constant between V_R and V_T characterising any given material [32]. Similarly, we can write $V_T = C_{TL}V_L$. Hence, one can easily deduce for crystalline Si [9] that $C_{RT} = 0.88$ and $C_{TL} = 0.694$. Since H-PS films are obtained from single crystal wafers, whose upper surfaces have been electrochemically treated, they should have similar atomic structure as that of their Si parent. We can then consider that the ratio of transverse and longitudinal velocities of silicon remains identical to that of its corresponding porous material, *i.e.* $(V_T/V_L)_{H-PS} \approx (V_T/V_L)_{c-Si} = 0.694$. Hence, introducing this value into relations (4) and (5) should lead to more accurate expressions of E and G as follows:

$$E = 0.997\rho V_L^2 , \qquad (10)$$

$$G = 0.482\rho V_L^2 . \qquad (11)$$

6.1.3. Validity of the proposed approaches

It is worth noting that the above deduced relations (8)–(11) are similar to those reported in literature [33]: $E = \rho V_L^2$ and $G = 0.38\rho V_L^2$. For G, the discrepancy in the proportionality constants for shear modulus, in relation (11) and that in ref. [33], is due to the fact that the latter case concerns the average of a whole range of materials, Poisson ratios of which vary from 0 to 0.5; it is then less accurate than that of relation (11) specifically derived for just one material, namely, silicon.

To test, even further, the validity of the introduced approximations we first apply the above derived relations (8)–(11) to single crystal Si and compare the deduced results of its elastic constants to those reported in literature. For p-type Si ⟨100⟩ with a density α_0 = = 2300 kg/m^3, all the results thus obtained are summarized in Table together with some published data [9, 10, 12, 34]. It is clear that the present results (E = 163.1 GPa and G = 70.3 GPa) are in agreement with literature; a close analysis shows that the best agreement is obtained with the approach specifically derived for porous silicon (relations (10) and (11)). Whereas, the general approach based on the Viktorov formula (relations (8) and (9)), though acceptable, leads to relatively smaller values (E = 158 GPa and G = = 70.3 GPa). Another test of relations (10) and (11) is the very good similarity between the deduced E/G ratios for c-Si (E/G = 2.08, in this work) and those determined from literature [34, 9]. Therefore, the application of the approach specifically derived for porous Si gives more accurate values. Hence, relations (10) and (11) can be safely used to obtain consistent results.

6.2. Evaluation of elastic constants of highly porous silicon and discussion

It is known that the density, ρ, of porous materials [9, 13, 20] is related to that of crystalline silicon, ρ_0, by the relation:

$$\rho = \rho_0(1 - P). \qquad (12)$$

© 2006, V. Lashkaryov Institute of Semiconductor Physics, National Academy of Sciences of Ukraine

Thus, the density of highly porous (80 %) silicon layers becomes $\rho = 460\ \text{kg/m}^3$. It is then possible to deduce both elastic constants, with a good accuracy, via the application of the optimal approach (relations (10) and (11)). The results obtained in this way for highly porous (80 %) *p*-type Si ⟨100⟩ are $E = 1.29$ GPa and $G = 0.63$ GPa (Table); the ratio of $(E/G)_{\text{H-PS}} = 2.06$ is similar to that of its crystalline parent $(E/G)_{\text{c-Si}} = 2.08$. These low values are typical of highly porous materials. It is worth noting that among elastic moduli of highly porous silicon only very rare values, to our knowledge, have been reported on Young's modulus [12, 13].

To compare the obtained results, let us consider the work of Bellet *et al*. [12] who put into evidence that Young's modulus varies not only with porosities but also with doping levels: E_p for *p*-type PS layers is smaller than E_{p+} for heavily doped p^+-type PS films. Quantitatively, it was reported for high porosity films (70 and 80 %) that: $(E_{p+})_{70\%} = 12$ GPa, $(E_p)_{70\%} = 2.4$ GPa and $(E_{p+})_{80\%} = 5.5$ GPa. Although, the *p*-type 80 % PS film (our case) was not included [12], its value should be smaller that of heavily doped PS layers, *i.e.*, $(E_p)_{80\%} < (E_{p+})_{80\%} < 5.5$ GPa; in agreement with this work: $(E_p)_{80\%} = 1.29$ GPa. Moreover, to improve this comparison, we deduce a value for Young's modulus of the 80 % porous silicon *p*-layer. In fact, by considering relations (1b) or (2b) that do not depend on doping, one can conclude that the ratio of Young's modulus between two different doping levels of a material (with the same parameter *n* and the same degree of porosity *P*) remains constant, so that:

$$(E_{p+}/E_p)_{P\%} \approx (E_{p+}/E_p)_{80\%} \approx (E_{p+}/E_p)_{70\%}. = \text{C}. \qquad (13)$$

Hence, by replacing known *E* values [12] one gets: $(E_{p+}/E_p)_{70\%} = 5$ corresponding to $E_{p+} = 5E_p$. Therefore, for the 80 % PS layers, it can be deduced that $(E_p)_{80\%} = 1.1$ GPa in good agreement with this work. Another comparison is the application of relation (1b) where the empirical parameter of porous silicon was reported to be $n = 2.95$ [13]; the value thus deduced is found to be $(E_p)_{80\%} = 1.3$ GPa, which compares very favourably with that obtained in Table.

Therefore, the present simple approach, based on expressing both elastic constants on just one acoustic parameter, V_L, not only can give good evaluation of Young's modulus (relation (10)) but can also be extended to shear modulus (relation (11)) that is found to be $G = 0.63$ GPa (Table). This approach is less complicated than Nielson model [35] concerning two-phase materials, which has been recently applied to porous oxide films [36]. Moreover, such a simple but accurate approach can be successfully applied to porous and non-porous materials, in particular to *slow* materials characterised by very low SAW velocities. It can also be useful in the determination of elastic moduli when using acoustic microscopes with small aperture lenses, which only generate leaky surface skimming longitudinal compressional waves [37].

Table. Elastic constants of single crystal Si and highly porous Si; the c-Si case is considered here to show the validity of the introduced approximations.

Materials	*E* (GPa)	*G* (GPa)	*E* /*G*	Source of *E* and *G*
Single crystal Si	158.8	70.30	2.25	Relations (8) and (9), this work
	163.1	78.80	2.08	Relations (10) and (11), this work
	165.5	79.70	2.08	Ref. [34]
	166.7	79.50	2.10	Ref. [9]
	165.3	–	–	Ref. [10]
	162.0	–	–	Ref. [12]
Highly porous (80 %) Si	1.25	0.56	2.23	Relations (8) and (9), this work
	1.29	0.63	2.06	Relations (10) and (11), this work
	1.10	–	–	Deduced from Ref. [12]
	1.30	–	–	Deduced from Ref. [13]

7. Conclusions

In conclusion, experimental $V(z)$ curves of highly (80 %) porous silicon films having different thicknesses were measured by SAM at variuos operating frequencies ($f = 58$, 142, and 565 MHz). Such signatures were either dominated by the substrate response or completely attenuated for higher thickness, from which a value of $\alpha_x = 0.2\ \mu\text{m}^{-1}$ was deduced. Moreover, two simple approaches for expressing elastic constants in terms of only longitudinal velocity were proposed. The best appropriate approximations, that compare favourably with conventional formula, were shown to be of the form: $E = 0.997\rho V_L^2$ and $G = 0.482\rho V_L^2$. The application of such formulae led to evaluation of both elastic moduli for this highly porous silicon, characterised by its RT electroluminescence; they were found to be $E = 1.29$ GPa and $G = 0.63$ GPa.

Acknowledgements

This work was, partly, carried out under l'acc. Program. Algéro-Français N°90 MDU 152 between LSC and LAMM.

References

1. C. Pickering, M.I.J. Beale, D.J. Robbins, P.J. Pearson and R. Greef, Optical studies of the structure of porous silicon films formed in p-type degenerate and non-degenerate silicon // *J. Phys. C: Solid State Phys.* **17** (35), p. 6535-6552 (1984).

© 2006, V. Lashkaryov Institute of Semiconductor Physics, National Academy of Sciences of Ukraine

2. L.T. Canham, Silicon quantum wire array fabrication by electrochemical and chemical dissolution of wafers // *Appl. Phys. Lett.* **57** (10), p. 1046-1048 (1990).
3. O. Bisi, S. Ossicini and L. Paresi, Porous silicon: a quantum sponge structure for silicon based optoelectronics // *Surf. Sci. Repts* **38**, p. 1-126 (2000).
4. L. Canham, *Properties of Porous Silicon*, INSPEC, IEE, London, 1997.
5. V. Lehman and U. Gosele, Porous silicon: Quantum sponge structures grown via a self-adjusting etching process // *Adv. Mater.* **4** (2), p. 114-116 (1992).
6. H. Mimura, T. Futagi, T. Matsumoto and Y. Kanimutsu, A visible light-emitting diode using a PN junction of porous silicon and microcrystalline silicon carbide // *J. Non-Cryst. Solids* **164-166**, p. 949-952 (1993).
7. Z.C. Feng and R. Tsu (Eds.), *Porous silicon*. World Scientific, NJ & London, 1994.
8. K. Barla, R. Herino, G. Pomchil and J.C. Pfister, Determination of lattice parameter and elastic properties of porous silicon by X-ray diffraction // *J. Cryst. Growth* **68** (3), p. 727-732 (1984).
9. Y. Boumaiza, Z. Hadjoub, A. Doghmane and L. Deboub, Porosity effects on different measured acoustic parameters of porous silicon // *J. Mater. Sci. Lett.* **18**, p. 295-297 (1999).
10. G.M. Da Fonseca, J.M. Saurel, A. Foucaran, and J. Camassel, E. Massone, T. Talierco and Y. Boumaiza, Acoustic investigation of porous silicon layers // *J. Mater. Sci.* **30,** p. 35-39 (1995).
11. G.M. Da Fonseca, J.M. Saurel, A. Foucaran, E. Massone, T. Talierco and J. Camassel, Acoustic microscopy invetigation of porous silicon // *Thin Solid Films* **225,** p. 155-158 (1995).
12. D. Bellet, P. Lamagère, A. Vincent and Y. Brechet, Nanoindentation investigation of the Young's modulus of porous silicon // *J. Appl. Phys.* **80** (7), p. 3772-3776 (1996).
13. H.J. Fan, M.H. Kuok, S.C. Ng, R. Boukherroub, J.-M. Baribeau, J.W. Fraser and D.J. Lockwood, Brillouin scattering of acoustic modes in porous silicon films // *Phys. Rev. B* **65**, p. 165330.1-8 (2002).
14. D.J. Lockwood, M.H. Kuok, S.C. Ng and Z.L. Rang, Surface and guided acoustic phonons in porous silicon // *Phys. Rev. B* **60** (12), p. 8878-8882 (1999).
15. G.T. Andrews, J. Zuk, H. Klefte, M.J. Clouter and E. Nossarzewska-Orlowska, Elastic characterization of a supported porous silicon layer by Brillouin scattering // *Appl. Phys. Lett.* **69** (9), p. 1217-1219 (1996).
16. M.G. Beghi, C.E. Bottani, G. Ghislouti, G. Amato and L. Boarino, Brillouin scattering of porous silicon // *Thin Solid Films* **297** (1/2), p. 110-113 (1997).
17. A. Briggs (ed.), *Advances in acoustic microscopy*, Plenum, New York, 1995.
18. A. Briggs, *Acoustic microscopy*, Clarendon, Oxford, 1992.
19. P.V. Zinin, Quantitative acoustic microscopy of solids (Chap. 8) in: *Handbook of elastic properties of solids, liquids and gases* / Eds. M. Levy, H.E. Bass and R.R. Stern, p. 187-226. Academic Press, New York, 2001.
20. K.K. Phani, S.K. Niyogi, A.K. Maitra and M. Roychaudhury, Strength and elastic modulus of a porous brittle solid: an acousto-ultrasonic study // *J. Mater. Sci.* **21**, p. 4335-4341 (1986).
21. V. Roque, B. Cros, D. Baron and P. Dehaudt, Effects of porosity in uranium dioxide on microacoustic and elastic properties // *J. Nucl. Mater*. **277**, p. 211-216 (2000).
22. A.K. Maitra and K.K. Phani, Ultrasonic evaluation of elastic parameters of sintered powder compacts // *J. Mater. Sci.* **29**, p. 4415-4419 (1994).
23. A. Halimaoui, C. Oules and G. Bomchil, Electroluminescence in the visible range during anodic oxidation of porous silicon films // *Appl. Phys. Lett.* **59** (3), p. 304-306 (1991).
24. J. Kushibiki and N. Chubachi, Material characterization by line-focus-beam acoustic microscopy // *IEEE Sonics Ultrason.* **SU-32**, p. 189-212 (1985).
25. A. Kulik, P. Richard, S. Sathish and G. Gremaud, Continuous wave transmission measuring scanning acoustic microscopy, in: *Acoustical Imaging* **19**, Eds. H. Ermert and H.-P. Harjes, p. 697-701. Plenum Press, New York, 1992.
26. A. Doghmane and Z. Hadjoub, Theoritical and experimental investigations of acoustic materials signatures via variable-illumination lens-stop system // *J. Phys. D: Appl. Phys.* **30**, p. 2777-2782 (1997).
27. A. Doghmane, Z. Hadjoub and F. Hadjoub, Nondestructive acoustic micro-characterisation of heteropolysiloxanes thin films // *Thin Solid Films*, **310**, p. 203-207 (1997).
28. Y.-C. Lee, J.D. Achenbach, M.J. Nystrom, S.R. Gilbert, B.A. Block and B.W. Wessels, Line-focus acoustic microscopy measurements of Nb_2O_5/MgO and $BaTiO_3$/$LaAlO_3$ thin-film/ substrate configurations // *IEEE Trans. Ultrason. Ferroelec. Freq. Control*. **42**, p. 376-380 (1995).
29. S. Bouhedja, I. Hadjoub, A. Doghmane and Z. Hadjoub, Investigation of Rayleigh wave attenuation via annular lenses in acoustic microscopy // *Phys. status solidi* (*a*) **202** (6), p. 1025-1032 (2005).
30. I.R. Smith and H.K. Wickramasinghe, SAW attenuation measurements in the acoustic microscope // *Electron. Lett.* **18** (22), p. 955-956 (1982).
31. L.A. Viktorov, *Rayleigh and Lamb Waves*. Plenum, New York, 1967.
32. F. Hadjoub, Z. Hadjoub, A. Gacem, I. Beldi and A. Doghmane, Surface tilting effects on elastic

© 2006, V. Lashkaryov Institute of Semiconductor Physics, National Academy of Sciences of Ukraine

constants in acoustic microscopy investigations // *Electron. Lett.* **34** (18), p. 1797-1799 (1998).

33. M.F. Ashby and D.R.H. Jones, *Matériaux: Propriétés et Applications*. Dunod, Paris, 1996.
34. Y-C. Lee, J.O. Kim and J.D. Achenbach, Acoustic microscopy measurements of elastic constants and mass density // *IEEE Trans. Ultrason. Ferroelec. Freq. Control*. **42**, p. 253-264 (1995).
35. L.F. Nielson, Elastic properties of two phase materials // *Mater. Sci. Eng.* **52**, p. 39-62 (1982).
36. P.V. Zinin, O. Lefeuvre, A. Briggs, B.D. Zeller, P. Cawley, A. Kinloch, X. Zhou, and G. Thompson, Determination of density and elastic constants of a thin phosphoric acid-anodized oxide film by acoustic microscopy // *J. Acoust. Soc. Amer.* **106** (5), p. 2560-2567 (1999).
37. Z. Hadjoub, K. Alami, A. Doghmane, J. M. Saurel and J. Attal, Acoustic microscopy skimming mode generation using small apertures lenses // *Electron. Lett.* **27** (11), p. 981-982 (1991).

© 2006, V. Lashkaryov Institute of Semiconductor Physics, National Academy of Sciences of Ukraine